Proceedings of the
International Conference on Mechanical Engineering 2009
(ICME2009) 26- 28 December 2009, Dhaka, Bangladesh

ICME09-FM-28

A MODIFIED EULERIAN-LAGRANGIAN APPROACH FOR SOLVING MULTI-PHASE FLOW APPLIED TO A COMPACT DOWN-HOLE SUB-SEA GAS-LIQUID SEPATATOR

Shakil Ahmed[1], **Gerardo Sanchez Soto**[1], **Jamal Naser**[2] **and Edson Nakagawa**[1]

[1]CSIRO Earth Science and Resource Engineering, Technology Park Kensington, Perth
[2]School of Engineering and Industrial Sciences, Swinburne University of Technology, Hawthorn, Melbourne

ABSTRACT

This paper presents a modified Eulerian-Lagrangian approach for solving multi-phase flow applied to a laboratory scale gas-liquid separator designed for high gas content. The separator consists of two concentric pipes with swirl tube in the annular space between the pipes. The gas-liquid mixture comes from the tangential side inlet and the system works with a combination of gravity and centrifugal forces to achieve a high-efficient gas-liquid separation. In the modified Eulerian-Lagrangian method, gas flow is coupled with the spray and wall film models. Spray model involves multi-phase flow phenomena and requires the numerical solution of conservation equations for the gas and the liquid phase simultaneously. With respect to the liquids phase, discrete droplet method (DDM) is used. The droplet-gas momentum exchange, droplet coalesces and breaks-up, droplet-wall interaction with wall-film generation and entrainment of the water droplet back into the gas stream are taken into account in this investigation. To be consistent with the experiments the same air water mixture is used for the present work. The standard k-ε turbulence model is used for turbulence closure. The predicted results from the modified Eulerian-Lagrangian multi-phase model explain the complex flow behavior inside the separator and are in good agreement when compared with experiments.

Keywords: Modified Eulerian-Lagrangian Approach, Compact Gas-liquid Separator, Multi-Phase Flow.

1. INTRODUCTION

The gas-liquid separation technology currently used by the petroleum industry is mostly based on the gravity driven vessel type separator which is large, heavy and expensive to purchase and operate especially in the subsea. This brought a lot of attention to academic researchers as well as field operators [1-4] to develop a compact gas-liquid separator suitable for off-shore application and potentially in sub-sea in order to enhance the recovery of the gas fields. A separator has to be simple, reliable with low maintenance requirements, minimal footprint, low pressure loss and easy to install. Considering all of these characteristics the swirl tube technology could be best suited to design a gas-liquid separator. Gas-liquid cylindrical cyclone separator (GLCC) and a gas-liquid separator being developed by CSIRO (CS-T) are excellent examples of designs for this kind of applications. GLCC has been implemented in a number of applications as reported recently by Kouba et al. [5]. Experimental data of GLCC operational envelope and a mechanistic model for GLCC separators have been reported by Arpandi el al. [6]. On the other hand laboratory scale experimental investigation has just been completed by Wong et al. [7] for the CSIRO's gas-liquid CS-T. However, more investigation is required to develop a mechanistic model for the gas-liquid CS-T.

Simulation of the flow behavior in GLCC separator applying a computational fluid dynamics (CFD) approach was presented for single-phase and two-phase flow by Erdal [8] and Erdal et al. [9]. Motta et al. [10] presented a simplified CFD model for rotational two-phase flow in a GLCC separator. The model assumes an axisymmetric flow and three velocity components, applicable to steady-state and isothermal conditions. Ahmed et al. [11] presented the numerical modeling of gas-liquid CS-T separator where they used Eulerian-Eulerian approach for modeling the complex behavior of the multi-phase flow. The predicted pressure drop, flow field and volume fraction were reasonably matched when compared with experiments. The presence of liquid droplets and a possible liquid film poses new challenges to the separation phenomena regarding the two-phase flow pattern and droplets break-up/ coalescence which cannot be modeled using Eulerian-Eulerian approach of multi-phase flow. Ahmed et al. [11] concluded in their paper to use a new modified Eulerian-Lagrangian approach with specific sub model for wall film and droplets break-up/coalescence and that is the motivation of this present work.

The current investigation presents a modified

Eulerian-Lagrangian approach for solving multi-phase flow applied to a laboratory scale gas-liquid separator designed for high gas content. The separator consists of two concentric pipes with helical swirl tube in the annular space between the pipes. The gas-liquid mixture enters tangentially from a side inlet into the separator and passes through the annular swirl tube. While passing through the swirl tube the liquid separates from the gas due to the centrifugal action, strikes at the inner wall of the outer pipe, and creates a liquid film at the wall, which ultimately descends due to gravity. On the other hand the lighter gas rises through the inner tube and the separation occurs with a combination of centrifugal force and gravity. The unique feature of the gas-liquid CS-T separator is its simple design without any moving parts. The performance of the gas-liquid CS-T separator is visually established by observing the liquid carry over (LCO) regime in which liquid is carried out in the gas stream. The liquid and gas flow rates at which the LCO is observed defines the upper operational range of the separator. To be consistent with the experiments, the same air-water mixture is used for the current numerical investigation.

2. NUMERICAL MODELING

Three-dimensional, transient and incompressible multiphase flow fields are obtained by solving the continuity and Navier-Stokes equations. The modified Eulerian-Lagrangian multiphase model is used where gas flow is coupled with the spray and wall film models available in commercial software FIRE [12]. Spray model involves multi-phase flow phenomena and requires the numerical solution of conservation equations for the gas and the liquid phase simultaneously. With respect to the liquid phase, discrete droplet method (DDM) is used. DDM operates by solving ordinary differential equations for the trajectory, momentum, heat and mass transfer of single droplet, each being a member of a group of identical non-interacting droplets termed a 'parcel'. Thus one member of the group represents the behavior of the complete parcel. Droplet parcels are introduced in the flow domain, along with the gas flow, with initial conditions of position, size, velocity, temperature and number of particles in the parcel. The droplet-gas momentum exchange, turbulent dispersion, secondary break-up, droplet collision and droplet-wall interaction are covered with a comprehensive set of models which allow the usage of the module very suitable for gas-liquid separation. The droplets are tracked in a Lagrangian way through the computational grid used for solving the gas phase partial differential equations. Full two-way coupling (interaction) between the gas and liquid phases is taken into account.

In a gas-liquid separator, a significant amount of the liquid can be deposited on the walls as a thin liquid film due to wall collisions of liquid. Some amount of this liquid is sheared off and entrained back into the gas flow. The coupling between the liquid film phase and the air flow is accomplished in FIRE by setting up modified and refined boundary conditions at the interface. At high air velocity, the shear force at the film surface tears droplets entrained back into the air flow. The wall film entrainment model is simulated within the wall film module. The governing equations used for DDM spray and wall film modeling are described in the following section.

2.1 DDM Spray Model

The governing equations for the trajectory and velocity of a particle parcel are as follows:

$$m_p \frac{du_{ip}}{dt} = F_{idr} + F_{ig} \tag{1}$$

where F_{idr} is the drag force, given by:

$$F_{idr} = D_p . u_{irel} \tag{2}$$

D_p is the drag function, defined as:

$$D_p = \frac{1}{2} \rho_g A_p C_D |u_{rel}| \tag{3}$$

C_D is the drag coefficient which generally is a function of the particle Reynolds number Re_p and A_p is the cross-sectional area of the particle. F_{ig} is a force including the effects of gravity and buoyancy and is given by:

$$F_{ig} = V_p . (\rho_p - \rho_g) g_i \tag{4}$$

Substituting the above forces in Eq. (1) the equation for the particle acceleration can be obtained and the integration of that equation will give the particle velocity.

2.2 Secondary Chu Break-up Model

The theoretical correlation is constructed in order to predict droplet sizes on the basis of an exponential function. The model implemented in this simulation represents a modified version of Chu's [13] original model in that it includes a Taylor-series expansion of the exponential term to first order, and subsequently an explicit discretization in time in which particle diameter correlation is written as:

$$\frac{dD}{dt} = -C_o . C_1 We^{C_2} (u_{rel} \varepsilon^{0.5}) T^{*(C_1 - 1)} \tag{5}$$

where C_0 is the function of the density ratio ε:

$$C_o = 0.1708 - 0.149\varepsilon^{0.5} \qquad \varepsilon = \rho_g / \rho_p \tag{6}$$

and T^* is a non-dimensional accumulated time within the particle integration time step when using sub-cycling method for solving Eq. (5).

$$T^* = \frac{\varepsilon^{0.5} u_{rel} t}{D_o} \tag{7}$$

The stable particle radius should exist if the critical Weber number We_{crit} is below 12

$$r_{stable} = \frac{2.We_{crit}\sigma}{\rho_g u_{rel}^2} \tag{8}$$

The values for the constants C_1 and C_2 used in this simulation are 0.772 and 0.246 respectively.

2.3 Schmidt-O'Rourke Coalescence Model

The Schmidt-O'Rourke coalescence model [14] performs the collision calculation for pairs of particles only if they are in the same computational cell. For description the particles with larger radius are called *collectors* and those with smaller radius are called *droplets*. The collision frequency ν between a particle of parcel 1 and all particles associated with another parcel,

within the computational volume, is used to calculate the probability *P* that a particle of parcel 1 will collide with a particle of the other parcel (pairs). The collision frequency ν of a *collector* with all (surrounding) *droplets* is calculated according to:

$$\nu = \frac{N_2}{V_{cell}} \frac{\pi}{4} (d_1 + d_2)^2 |u_1 - u_2| \quad (9)$$

the subscripts 1 and 2 refer to the properties of the *collectors* and *droplets* respectively. N_2 is the number of particles in parcel 2 and V_{cell} is the volume of the computational cell in which both parcels are located. The probability *P* that a *collector* undergoes *n* collisions with *droplets* follows a Poisson distribution:

$$P_n = e^{-\bar{n}} \frac{\bar{n}^n}{n!} \quad (10)$$

with the mean value (number of expected collisions) $\bar{n} = \nu.\Delta t$, where Δt is the computational time step. Thus the probability of no collisions is $P_0 = e^{-\bar{n}}$. A random number R_{n1} in the range $0 \le R_{n1} \le 1$ is then used to decide whether a collision takes place or not. If $R_{n1} < P_0$ then no collisions are calculated for the particular pair of particles in associated parcels. If $R_{n1} \ge P_0$ then all the *collectors* will undergo one or more collisions with the *droplets*, where each collision is of the same type.

In the case of collisions a second random number R_{n2} also in the range $0 \le R_{n2} \le 1$ is used to determine which type of collision takes place. For this, a collision impact parameter is defined as:

$$b = (d_1 + d_2)\sqrt{R_{n2}} \quad (11)$$

if $b < b_{cr}$, where b_{cr} is the critical impact parameter below which coalescence may occur, then the result of every collision is coalescence. If $b \ge b_{cr}$, then each collision is a grazing collision, i.e. the particles maintain their sizes and temperature but undergo velocity changes. The value of b_{cr} depends on the particle diameter, the relative velocity between the particles and the liquid surface tension coefficient:

$$b_{cr}^2 = (d_1 - d_2)^2 \min[1.0,\ 2.4(f(\gamma)/We_d)] \quad (12)$$

$$f(\gamma) = \gamma^3 - 2.4\gamma^2 + 2.7\gamma, \quad \gamma = \frac{d_2}{d_1} \quad d_2 > d_1 \quad (13)$$

$$We_d = \frac{\rho_p |u_{d1} - u_{d2}|^2}{2\sigma} d_1 \quad (14)$$

the random number R_{n2} is used to determine the number of coalescences *n* for each *collector*:

$$\sum_{k=0}^{n-1} P_k \le R_{n2} < \sum_{k=0}^{n} P_k \quad (15)$$

for each *collector* particle, *n droplets* are removed from their associated parcel and the properties of the *collector* particles, diameter, velocity and temperature are appropriately modified due to conservation of mass, momentum and energy. If there are an insufficient number of *droplets* to have *n* coalescences with the *collector*, then *n* is recomputed so that all N_2 *droplets* coalesce, and the parcel associated with the *droplets* is removed from the calculation.

In the case of grazing collision, only one collision is calculated for each particle. Grazing collisions are calculated between *N* pairs of particles, where *N* is the minimum of N_1 and N_2. The *N collectors* and *droplets* are then return to their parcels in such a way that mass, momentum and energy are conserved. The expression giving the velocity of each particle after a collision is:

$$u_{d1}^* = \frac{u_{d1} d_1^3 + u_{d2} d_2^3 + d_2^3 (u_{d1} - u_{d2}) R_{n3}}{d_1^3 + d_2^3} \quad (16)$$

where R_{n3} is a further random number defined as:

$$R_{n3} = \frac{b - b_{cr}}{(d_1^3 + d_2^3) - b_{cr}} \quad (17)$$

2.4 Particle Wall Interaction/Splashing Model

The splashing model used for particle wall interaction is heavily based on systematic empirical investigations carried out with a wide variety of initial conditions. The predominant influence of particle momentum and properties such as viscosity and surface tension is taken into consideration by introducing the dimensionless groups Reynolds number and Ohnesorge number for the particular particle:

$$\mathrm{Re}_D = \frac{\rho d_0 u_{\perp 0}}{\mu} \quad (18)$$

$$Oh = \frac{\mu}{\sqrt{\rho \sigma d_0}} \quad (19)$$

the Reynolds number compares momentum to viscous forces, whereas the Ohnesorge number relates viscous forces to surface tension. For the Reynolds number, only the wall normal component $u_{\perp 0}$ of the initial particle velocity u_0 is used, which accounts for impact angle effects. Additionally, a K-value is defined as:

$$K = Oh.\mathrm{Re}_D^{1.25} \quad (20)$$

this *K*-value is used as the key parameter for the splashing model. The criterion for inception of splashing is given at *K*=57.7. Consequently, for *K*<57.7 the particles are deposited completely at the wall without bouncing or breakup. The kinetic energy of the particle is dissipated.

2.5 Wall Film Model

The basic governing equation for wall film flow is the film thickness equation. It is a slightly modified formulation of the continuity equation, which is transformed to conservation of film thickness. For simplicity, just the Cartesian formulation is presented here, but the wall film model is capable of dealing with distorted cells as well.

$$\frac{\partial \delta}{\partial t} + \frac{\partial \delta u_1}{\partial x_1} + \frac{\partial \delta u_2}{\partial x_2} = \frac{1}{\rho A}(S_{mD} - S_{mV}) \quad (21)$$

Instead of employing the momentum equations for solving the velocity components u_1 and u_2, wall film model uses the analytical film velocity profiles developed by AVL and implemented in FIRE [12]. If the velocity components as well as the source term S_m are known then the convection terms $\frac{\partial \delta u_1}{\partial x_1}$ and $\frac{\partial \delta u_2}{\partial x_2}$ can be evaluated and Eq. (21) can immediately be solved explicitly.

2.6 Wall Film Entrainment Model

The entrainment model used in this simulation is the Schadel-Hanratty model [15] where the critical Weber number, specifying the onset of entrainment is defined as:

$$We_{cr,SH} = \frac{\rho_g u_{rel}^2 \delta}{\sigma} \quad (22)$$

and the limit is set to We_{cr}=17.0. The relative velocity u_{rel} is:

$$u_{rel} = \left| \bar{u}_{gas} - \bar{u}_f \right| \quad (23)$$

the model calculates the entrainment rate as the amount of mass sheared off the film per unit area and unit time according to the Eq. (24).

$$R_{A,SH} = X_{RA} u_\tau \sqrt{\rho_g \rho_f}.10^{-3} \quad [\text{kg/m}^2\text{s}] \quad (24)$$

where:

$$X_{RA} = 0.4.\ln(150.I_R.We_{SH} + 1) + 1.4\sqrt{I_R.We_{SH}} \quad (25)$$

with the roll wave intermittence factor as a function of excess film flow rate Γ_E:

$$I_R = 0.15 + 0.75\Gamma_E \qquad I_R \le 0.5 \quad (26)$$

In Eq. (25) an alternative definition of Weber number is used by replacing relative velocity with friction velocity u_τ:

$$We_{SH} = \frac{\rho_g u_\tau^2 \delta}{\sigma} \quad (27)$$

the mass ripped off the film per unit area per unit time acts as a mass sink to the film and consequently as a mass source to the spray DDM. To introduce these new particles to the spray, particle diameter is calculated by Kataoka droplet correlation model [16] where a volume mean diameter is defined as:

$$D_{vm,K} = 0.028 \frac{\sigma}{\rho_g \bar{u}_g^2} \text{Re}_{f,IM}^{-1/3} \text{Re}_g^{2/3} \left(\frac{\rho_g}{\rho_f} \right)^{-1/3} \left(\frac{\mu_g}{\mu_f} \right)^{2/3} \quad (28)$$

with the film Reynolds number

$$\text{Re}_{f,IM} = \frac{4\bar{u}_f \delta \rho_f}{\mu_f} \quad (29)$$

3. BOUNDARY CONDITIONS AND MESH

The inlet boundary condition is set by introducing flow rates for both air and water at the tangential side inlet. The top outlet of the inner pipe, from where the air comes out after separation, is open to atmosphere in the experiments. So a pressure boundary condition is applied in the numerical simulation and the atmospheric pressure is set to 10^5 Pa. Experimental investigation reveals that gas (1-5%) in the form of bubbles is trapped and discharged with the downward flowing liquid. This phenomenon is known as gas carry under (GCU). GCU boundary condition is imposed at the bottom outlet of the outer pipe by assuming that 1% of the total gas is trapped as bubbles in the liquid flowing downward along the wall of the outer pipe.

The volume mesh consists of hexahedral elements. The solutions are grid independent when the total number of elements is 651,975. The interval step used for this simulation is 0.0025 s. The simulation was run until the solution had reached the steady-state. The convergence criterion for the momentum equations and turbulent parameters are 10^{-4} and for the continuity equation is 10^{-3}.

4. RESULTS AND DISCUSSIONS

The modified Eulerian-Lagrangian approach of multi-phase flow with specific sub-models for wall film and droplets break-up/coalescence is applied to gas-liquid CS-T separator. Two points, one on the experimental LCO curve (point 1) and one above (point 2) are selected for the simulations (Fig 1). For the point 1, an air flow rate of 383 L/min and water flow rate of 25 L/min are used. The air flow rate is then increased by 20% for point 2. The modeling is carried out in transient or time dependent fashion and hence the results presented represent a snapshot in time.

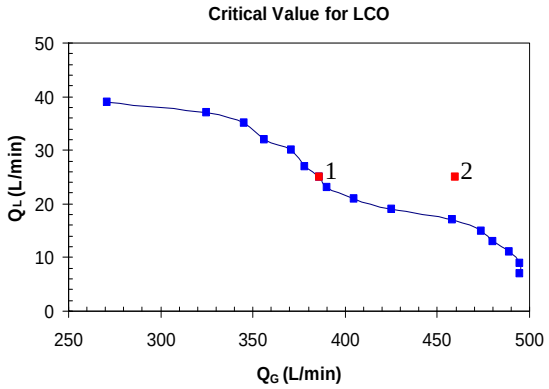

Fig 1. Two points for which simulations are performed

Velocity streamlines showing the flow path of air and velocity in the near wall regions for the point 1 are shown in Fig 2(a) and 2(b).

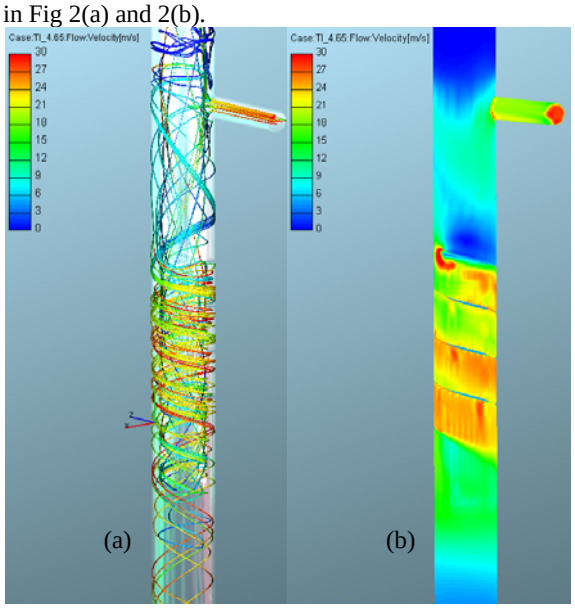

Fig 2. (a) Velocity streamlines showing the flow path of air and (b) velocity in the near wall regions for the point 1

The air-water mixture enters the annular space of the separator from the tangential inlet and strikes at the outer pipe. It then accelerates and moves downward towards

the swirl tube and reaches the maximum velocity (30 m/s) at the entrance of the swirl tube. The velocity then decreases to 25 m/s (Fig 2(b)) and almost constant inside the swirl tube. While passing through the swirl tube, the water gets separated from the air due to the centrifugal action and creates a liquid wall film at the outer pipe, which ultimately descends due to gravity. The lighter air rises, travels through the inner pipe and comes out from the air outlet.

Figure 3(a-b) shows the formation of the wall film by the spray droplets impinging on the outer pipe wall for point 1.

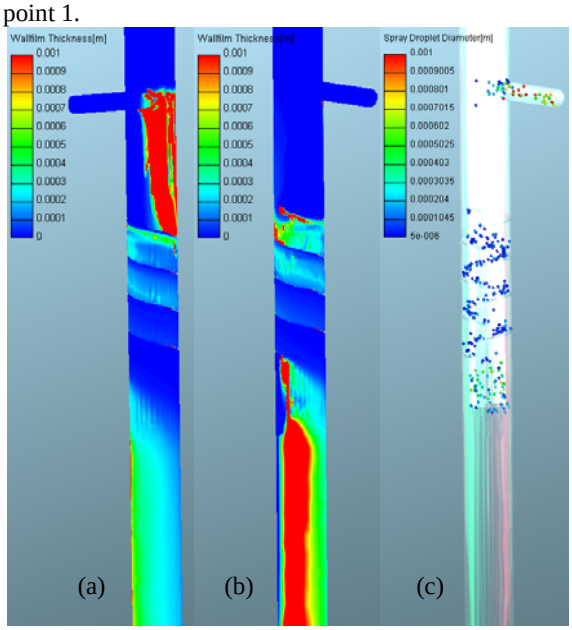

Fig 3. (a-b) Formation of the wall film by the spray droplets impinging at the outer pipe wall and (c) entrainment of the water droplets back into the air stream inside the swirl tube and at the entrance of the inner pipe

As the air-water mixture strikes the outer pipe wall in the annular space, most of the water droplets convert into wall film as shown in Fig 3(a). This wall film then moves downward towards the swirl tube. Inside the swirl tube the wall film thickness reduces and the entrainment of the water droplets back into the air stream occurs (Fig 3(c)). This phenomenon is more important at the entrance of the inner pipe where most of the water droplets along the periphery of the inner pipe coalesce, get bigger, and ultimately go down due to gravity. Only a couple of them are carried into the inner pipe due to the higher drag force dominating over the gravity and occasionally come out through the air outlet. This is the onset of LCO state which is captured in the simulation and consistent with the experiments. The size of the droplets is exaggerated in Fig 3(c) for visual comfort. The actual size of the droplet can be obtained from the color key. Each droplet represents a cluster of droplets or one member of the group or parcel. The wall film at the exit of the swirl tube moves downward (Fig 3(b)) along the outer pipe of the separator and thus the separation of the air-water mixture is completed.

The LCO curve shown in Fig 1 defines the upper operational range of the separator which indicates that for a point above this curve, a constant LCO occurs. To gain more confidence in this new approach another point (point 2) is simulated above the LCO curve, where the air flow rate is increased by 20% (459 L/min), and the results are explained in the next section.

Figure 4(a-b) shows the velocity in the near wall regions and wall film generation for the point 2. As expected, like point 1, the maximum velocity occurs (Fig 4(a)) at the entrance of the swirl tube but the magnitude is higher than the point 1 (36 m/s) because of increased air flow rate. No significant change occurs in the wall film formation between the point 1 and 2 (Fig 3(a-b) and 4(b)) as the water flow rate is same for both cases but the difference is clear when the LCO are compared.

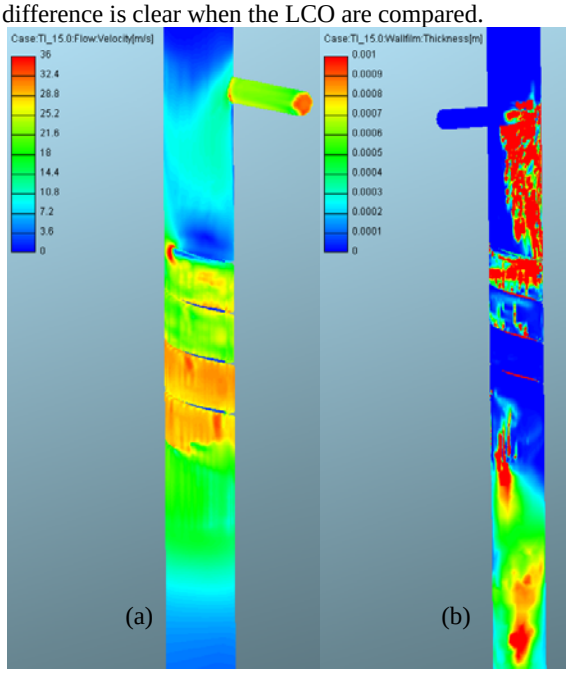

Fig 4. (a) Velocity in the near wall regions and (b) formation of the wall film for the point 2

Figure 5(a-b) compares the LCO in the inner pipe for the point 1 and 2. Point 1 represents the onset of LCO state where at the entrance of the inner pipe the water droplets are in unstable condition. At this region an increase in drag force over gravity carries a couple of droplets inside the inner pipe and ultimately through the air outlet. On the other hand point 2 is well above the LCO curve. An increase in air flow rate (20%) results in higher tangential velocity inside the swirl tube. Lots of water droplets are entrained back into the air stream in side the swirl tube due to the high shearing action between the wall film and the tangential air velocity. At the exit of the swirl tube air stream carries most of these water droplets in the inner pipe and a constant LCO occurs. This phenomenon is well captured in the simulation and consistent with the experiments.

5. SUMMARY AND CONCLUSIONS

This paper presents a modified Eulerian-Lagrangian approach for solving the complex multi-phase flow. The air flow was coupled with the spray droplets, wall film, break-up/coalescence and wall film entrainment model available in commercial software FIRE. The multi-phase model is applied to a gas-liquid CS-T separator to

understand the complex flow behavior inside it.

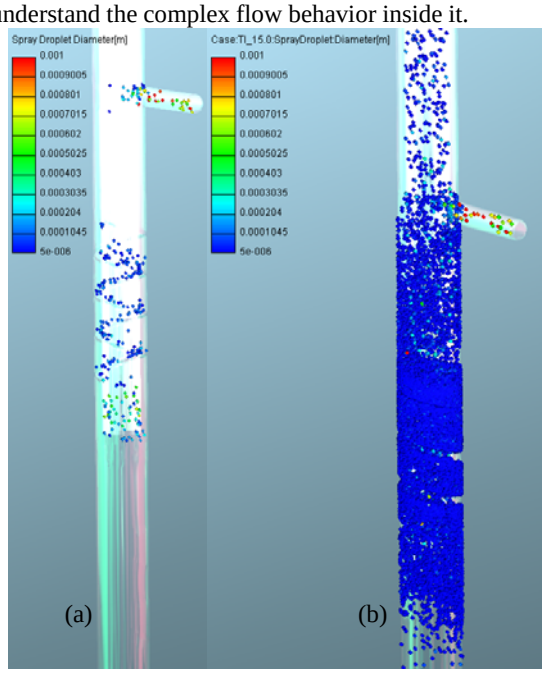

Fig 5. (a) Onset of LCO state for the point 1 shows unstable water droplets at the entrance of the inner pipe and (b) Increased air flow rate for the point 2 shows lots of water droplets in the inner pipe

The simulations are performed for two points: one on the experimental LCO curve (point 1) and the other well above the LCO curve (point 2). The onset of the LCO state is visually observed for the point 1. The air-water mixture is introduced into the separator from a tangentially side inlet and strikes the outer wall in the annular space where all the water droplets form the wall film. The wall film moves downward towards the swirl tube and passes through it. The thickness of the wall film reduces inside the swirl tube and due to the high tangential velocity, the shear force at the film surface tears droplets entrained back into the air flow. The entrainment phenomenon is more important at the entrance of the inner pipe, where all the water droplets are in unstable condition and a small increase in the drag force over the gravity results in LCO at the air outlet. The whole physics is well captured in this simulation and consistent with the experiment. The point 2 is well above the upper operating range of the LCO curve which indicates a constant LCO. The simulation of the point 2 shows (Fig 5(b)) a constant LCO and consistent with the experiment. This modified Eulerian-Lagrangian model can now be used to understand the flow phenomenon for complex multi-phase flow like gas-liquid CS-T separator

6. ACKNOWLEDGEMENTS

The authors gratefully acknowledge the financial and other support received for this research from the Western Australian Energy Research Alliance (WA: ERA) and Chevron Energy Technology Pty Ltd.

7. REFERENCES

1. Powers, M.L., 1993, “New perspective on oil and gas separation performance”, SFE prod. & facilities, pp. 15: 77-83
2. Talavera, P.G., 1990, “Selecting gas/liquid separator”, Hydrocarbon Process, pp. 10: 80-85
3. Choi, M.S., 1990, “Prediction of separator performance under changing field conditions”, Annual Technical Conference and Exhibition, Sep. 23-26, New Orleans, LA, SPE 20703
4. Noui-Mehidi, M.N., Wu, J., Cueille, P.V., Sanchez-Soto, G., Rivero, M. and Nakagawa, E., 2007, “Effect of Salinity on the performance of Gas Liquid Cyclonic Separators”, AIChE Journal, October, 53 (10), 2722-2725
5. Kouba, G., Wang, S., Gomez, L., Mohan, R., Shoham, O., 2006, “Review of the state-of-the-art gas/liquid cylindrical cyclone (GLCC) technology-field applications”, SPE J. Dec., SPE 104256
6. Arpandi, I. A., Joshi, A.R., Shoham, O., Shirazi, S., and Kouba, G.E., 1996, “Hydrodynamics of two-phase flow in gas-liquid cylindrical cyclone separators”, SPEJ, December, pp: 427-436
7. Wong, C.Y., Wu, J., Graham, L., Ahmed, S., Bowditch, P., Kilpatrick, T., and Sanchez-Soto, G., 2009, “Optimization of the CS-T gas-liquid separator- Final Report”, Confidential, CSIRO Material Science and Engineering (C), Highett, Melbourne, Australia
8. Erdal, F. M., 1996, “CFD simulation of single-phase and two-phase flow in gas-liquid cylindrical cyclone separator,” M.S. thesis, The University of Tulsa
9. Erdal, F. M., Shirazi, S. A., Shoham, O., and Kouba, G.E., 1996, “CFD simulation of single-phase and two-phase flow in gas-liquid cylindrical cyclone separator”, 71st SPE Annual Meeting, Denver, CO, October 6-9, SPE paper: SPE 36645
10. Motta, B.R.F., Erdal, F.M., Shirazi, S.A., Shoham, O., and Rhyne, L.D., 1997, “Simulation of single-phase and two-phase flow in gas-liquid cylindrical cyclone separators”, Proceedings of the ASME Summer Meeting, Vancouver, Canada, June 22-26, FEDSM97-3554
11. Ahmed, S., Noui-Mehidi, M.N., Naser, J., Sanchez-Soto, G., and Nakagawa, E., 2009, “Evaluation of numerical modeling for a compact down-hole sub-sea gas-liquid separator for high gas content”, APPEA Journal, pp: 433-440
12. Fire, Version 8, 2006, CFD Solver V8.5-Multiphase flow, Spray and Wall film Modeling
13. Chu, Cho-Chone C., 1986, “One-dimensional transient fluid model for fuel-coolant interaction analysis”, Thesis, University of Wisconsin-Madison
14. O’Rourke, P.J., 1989, “Statistical properties and numerical implementation of a model for droplet dispersion in turbulent gas”, J. Comput. Physics, 83
15. Schadel, S. A. and Hanratty, T.J., 1989, “Interpretation of atomization rates of the liquid film in gas-liquid annular flow”, Int. J. Multiphase Flow, 15 (6), pp. 893-900